Nanoenergy Communications
https://www.sciltp.com/journals/nc

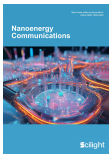

Mini Review

Recent Advances in Current-Amplification Strategies of Triboelectric Nanogenerators by Regulating Air Breakdown Effect

Seh-Hoon Chung and Sangmin Lee *

School of Mechanical Engineering, Chung-Ang University, Seoul 06974, Republic of Korea; slee98@cau.ac.kr

How To Cite: Chung, S.-H.; Lee, S. Recent Advances in Current-Amplification Strategies of Triboelectric Nanogenerators by Regulating Air Breakdown Effect. *Nanoenergy Communications* **2026**, *1*(1), 5.

Received: 16 January 2026
Revised: 11 February 2026
Accepted: 27 February 2026
Published: 9 March 2026

Abstract: Triboelectric nanogenerators (TENGs) are promising energy-harvesting devices that convert mechanical energy to electrical energy. Despite their many advantages, many TENGs generate a low current output owing to their limited surface charge density and charge transfer capacity, which limits their practical application. In this review, we introduce several strategies that can amplify the current output of TENGs by improving the surface charge density of the triboelectric layer using liquid lubricants, controlling atmospheric conditions, and increasing the charge transfer capacity via the electron avalanche effect from electrostatic discharges. We also provide useful insights and design guidelines for TENG amplification.

Keywords: triboelectric nanogenerators; current amplification; liquid lubricants; atmosphere control; electron avalanche

1. Introduction

With the rapid development of industry, energy demand and consumption have increased, leading to a need for renewable and clean energy sources that cause minimal environmental problems. In particular, the rapid advancement of artificial intelligence (AI) has resulted in the use of a large number of Internet of Things (IoT) sensor networks for various AI-driven applications, thereby increasing energy demand. Many researchers have focused on developing self-powered energy sources for IoT sensors, such as triboelectric nanogenerators (TENGs) [1–7], piezoelectric nanogenerators (PENGs) [8–10], and thermoelectric nanogenerators [11–13]. Among these technologies, TENGs have recently attracted considerable attention owing to their ability to harvest various types of mechanical energy, including human motion [14–18], wind energy [19–24], and hydro energy [25–31]. Moreover, TENGs offer advantages such as broad material selection [32–34], lightweight structure [35–38], low cost [39–41], and high output under low-frequency mechanical input [42–45]. Consequently, many researchers have studied the potential application of TENGs in biosensors [46–49], power sources for portable devices [50–52], and environmental monitoring devices [53–56].

According to the fundamental working mechanism, the coupling of triboelectrification and electrostatic induction is responsible for electricity generation in TENGs [57]. In TENGs composed of two separated electrodes with two different triboelectric materials attached to their surfaces, surface charge is transferred between the triboelectric materials during contact and separation. When the two plates are separated, the oppositely charged surfaces of the triboelectric materials induce opposite charges within the electrodes, driving the electrons to flow between the electrodes through an external circuit and generating an electric current. When the two plates come into contact again, the charges induced inside the electrodes are redistributed to reach an electrostatic equilibrium between the triboelectric materials. Owing to this cyclic process, TENGs can generate alternating current outputs.

However, despite this fundamental working mechanism, many TENGs still exhibit intrinsically low current outputs, typically in the nanoampere-to-microampere range, restricting their use as primary power sources. This

limitation arises primarily owing to two fundamental factors. The first is the limited surface charge density imposed by the air breakdown effect [58]. According to Paschen's law, electrical breakdown in air occurs when the electric field strength reaches several kilovolts per millimeter under dry air conditions. Consequently, even though the surface charge density of the triboelectric layers can be increased during TENG operation, the charges are released through air, which limits the electrical output. The second factor is the limited charge transfer by the electrostatic induction-dominated working mechanism. In such cases, the amount of charge transferred through the external circuit per cycle is constrained by the surface charge density of the triboelectric layers, resulting in an inherently low current output. Therefore, effective current amplification in TENGs requires strategies that overcome the limitations of surface charge density and charge transfer capacity.

In this review, we introduce recent advances in the current amplification of TENGs that overcome the limitations of surface charge density and charge transfer capacity as shown in Figure 1. The review focuses on new strategies to enhance current output by increasing surface charge density by regulating the surrounding conditions, such as using lubricant oil or vacuum conditions to increase the surface charge density. In addition, we introduce novel strategies that harness the electron avalanche effect during TENG operation, which can effectively increase the charge transfer capacity. This review will first discuss about enhancing surface charge by regulating the surrounding conditions of TENGs and introduce the high performance ESD based TENGs that can generate high power output with electron avalanche effect. Finally, the remaining challenges and future perspectives for further enhancing the current output of TENGs are discussed.

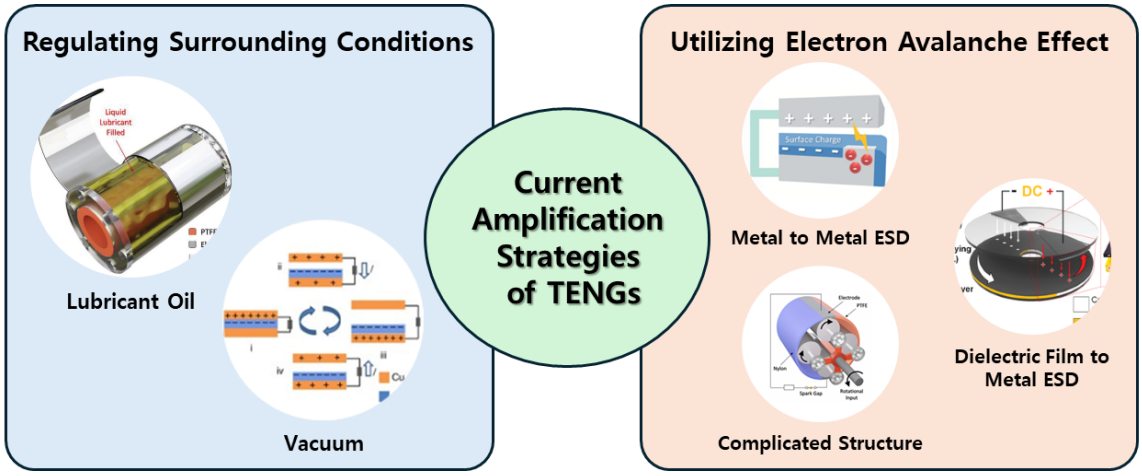

Figure 1. Overview of the current amplification strategies of TENGs.

2. Suppressing Surface Charge of Triboelectric Layers by Regulating the Surrounding Conditions

Triboelectrification was first described in ancient times. However, the mechanism of charge transfer during contact electrification remains controversial. Although many researchers have proposed different theories, currently, no unified model that can explain triboelectrification exists [59–62]. Nevertheless, for the selection of TENGs materials, accurate values of the surface charge density of each material are necessary to optimize the TENG structure [63,64]. Many researchers have calculated the surface charge density using experimental results.

Even though the surface charge density can be calculated based on experimental results, the amount of surface charge density could be limited by the surrounding conditions. According to Paschen's law, the threshold voltage for the gas breakdown can be described by the following equation:

$$V_b = \frac{Bpd}{\ln(Apd) - \ln[\ln(1 + \frac{1}{\gamma_{se}})]} \quad (1)$$

where V_b is the threshold breakdown voltage, p is the pressure, d is the gap distance between the electrodes. And the constant γ_{se} is the secondary electron emission coefficient, the constant A is the saturation ionization in the gas, and the constant B is related to the excitation and ionization energies. If d is 0.01 m, V_b can be calculated to be 36,142 V [65]. According to Zi et al., the surface charge density is limited to approximately 40–50 μC/m^2 owing to the gas breakdown effect arising from V_b. Therefore, it is unnecessary to reduce the air breakdown effect, which limits the electrical output of TENGs.

Several studies have reported the suppression of the air breakdown effect by controlling the surrounding environment of TENG devices. Figure 2 shows TENGs that generate a higher current output using lubricant oil. As shown in Figure 2a, Zhou et al. [66] demonstrated that the output performance of a freestanding sliding TENG (FS-TENG) can be enhanced using a liquid lubricant. As shown in Figure 2b, both the transferred charge and current output increased by more than 2.5-fold, from approximately 70 to 160 nC and from 0.2 to 0.36 μA, respectively. This output enhancement of the FS-TENG with the liquid lubricant was caused by the absence of the air breakdown effect, as shown in Figure 2c. Furthermore, the finite element simulation results shown in Figure 2d reveal that a lower electric field is generated under liquid lubricant conditions compared with air, indicating effective suppression of the air breakdown effect.

In addition, Chung et al. [67] demonstrated a nonpolar liquid-lubricant-submerged TENG (LLS-TENG), which enhances the current output via a liquid lubricant. The LLS-TENG was designed to completely fill the liquid lubricant inside the device, and the electrical output was generated by the rotation of the polytetrafluoroethylene (PTFE) cylinder and rolling electrodes. As shown in Figure 2f, the peak voltage and current outputs of the LLS-TENG increased from 28 to 200 V and 5 to 85 mA, respectively, using a liquid lubricant. Researchers have described that the current enhancement of the LLS-TENG with a liquid lubricant is caused by suppressing the field emission effect, which is also similar to the air breakdown effect, as the charges from triboelectrification are also released into the air, as shown in Figure 2g. Moreover, researchers have simulated the electric field strength between electrodes with the same geometry, as shown in Figure 2h, and determined that the electric field strength in the lubricant is weaker than that in air.

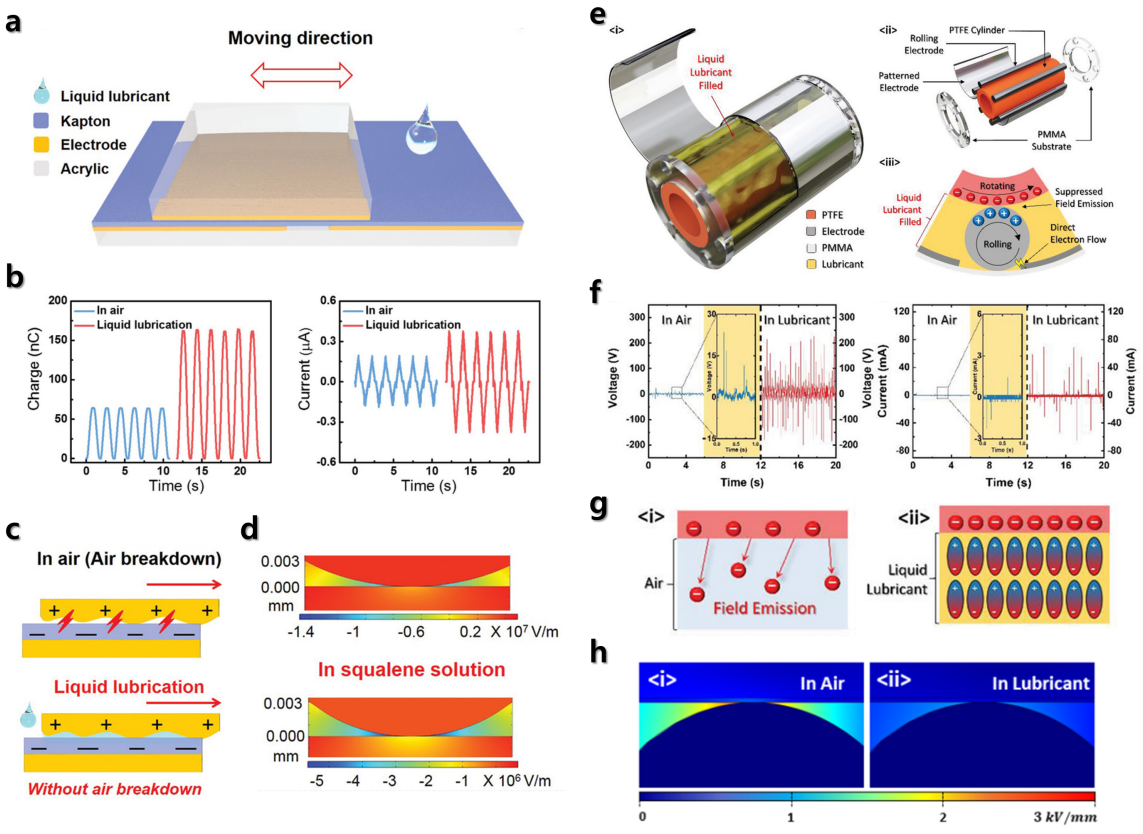

Figure 2. Using liquid lubricants to suppress surface charge density in TENGs. (**a**) Schematic of a FS-TENG using liquid lubricant [66], Copyright 2020, John Wiley and Sons. (**b**) Transferred charge and current output of FS-TENG. (**c**) Schematic of the role of liquid lubricant in FS-TENG. (**d**) Simulation results of electric field strength with and without liquid lubricant in FS-TENG. (**e**) Schematic of LLS-TENG [67], Copyright 2021, John Wiley and Sons. (**f**) Voltage and current outputs of LLS-TENG with and without liquid lubricant. (**g**) Schematic showing the role of the liquid lubricant in LLS-TENG. (**h**) Simulation results of electric field strength with and without liquid lubricant in LLS-TENG.

Figure 3 shows the experimental results, which reveal that the liquid lubricant was capable of suppressing the air breakdown effect and enhancing the electrical output of the TENGs. As shown in Figure 3a, Chung et al. [67] reported that the factors for enhancing the electrical output of TENGs include not only suppressing the surface

charge but also the large distance of the electrical double layer (EDL) of liquid lubricants. Thus, because polar liquids have smaller EDLs than nonpolar liquids, nonpolar liquids can enhance the electrical output of TENGs. As shown in Figure 3b,c, the voltage and current outputs of the LLS-TENG were measured when different liquids such as mineral oil (MO), silicone oil, castor oil, water (H_2O), and ethyl alcohol (EtOH) were used. The highest output was generated with MO, and no measurable output was generated with water or EtOH. Because the Debye lengths of H_2O and EtOH are significantly smaller than those of nonpolar liquids, this result shows that the Debye length of the liquid lubricant is one of the main factors for enhancing the electrical output of TENGs.

Wu et al. [68] reported that the relative permittivity of liquid lubricants is important for enhancing the electrical output of TENGs. As shown in Figure 3d,e, several lubricants, such as squalane, paraffin oil, and PAO 10, can enhance the voltage and current outputs of the TENG compared with dry air conditions. In addition, as shown in Figure 3f, the researchers described that one of the main factors affecting the electrical output enhancement of TENGs with liquid lubricants is the relative permittivity of the lubricants, owing to their stronger electron-donating capability and improved capacitance. Because liquid lubricants can be polarized and induce more charges with high permittivity, liquid lubricants with high permittivity are necessary to enhance the electrical output of TENGs. As shown in Figure 3f, the researchers investigated the permittivity of several lubricants and measured the voltage outputs of TENG by using these lubricants. As a result, a nonlinear relationship between the relative permittivity and voltage output was observed, as shown in Figure 3f.

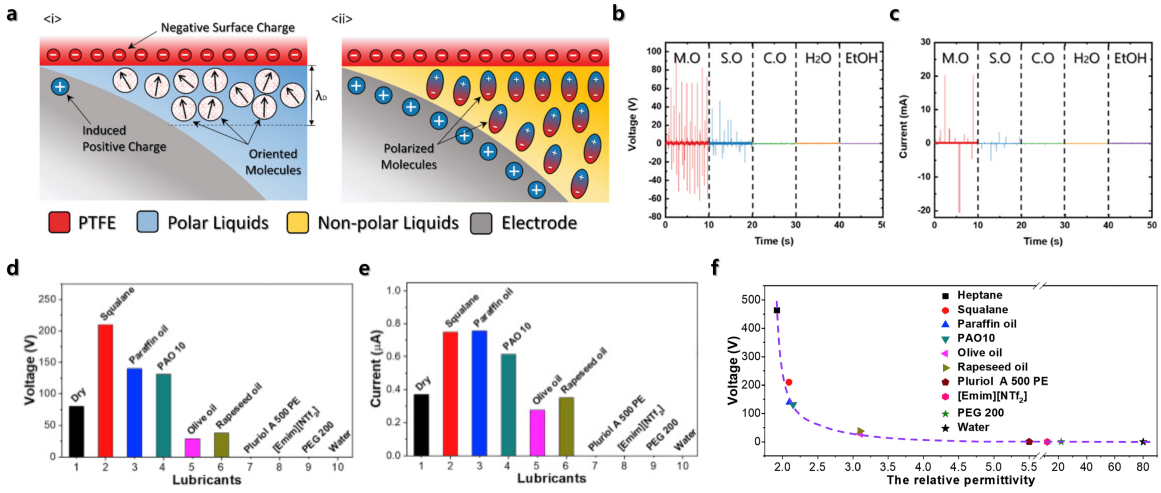

Figure 3. Detailed mechanism of liquid-lubricant-based TENGs and screening of various liquid lubricants. (**a**) Schematic showing the detailed working mechanism of liquid lubricant in LLS-TENG [67], Copyright 2021, John Wiley and Sons. (**b**) Voltage outputs of LLS-TENG with various liquid lubricants. (**c**) Current outputs of LLS-TENG with various liquid lubricants. (**d**) Voltage outputs with various liquid lubricants for sliding TENG [68]. (**e**) Current outputs with various liquid lubricants for sliding TENG. (**f**) Relationship between voltage and the relative permittivity of liquid lubricants.

In addition, the current output of TENGs can be enhanced by controlling the atmosphere, as shown in Figure 4. If the air breakdown voltage is increased by controlling the atmosphere, the limitation of the surface charge density of the triboelectric layers can be increased; thus, both the voltage and current outputs of TENGs can be increased. According to Wang et al. [69], the electrical output is enhanced under vacuum conditions by removing the surface charge released through air. Because there is no air under vacuum, charge release through air can be blocked. As shown in Figure 4a, the gas breakdown voltage by high charge density of TENGs can be higher than the gas breakdown voltage at short gap distance in 1 atm air condition, however, the gas breakdown voltage by high charge density of TENGs is higher than the gas breakdown voltage at large gap distance in 10^{-4} air atm condition. This means that lower pressure air condition can reduce gas breakdown effect of triboelectric layers. In addition, for the TENG device constructed as shown in Figure 4b, the charge density and current output were measured to be 120 μC/m^2 and 60 mA/m^2, respectively, under air. However, under vacuum conditions, the charge density and current output of the TENG device increased up to 660 μC/m^2 and 300 mA/m^2, as shown in Figure 4c,d, respectively. With this device, the TENG device under air and vacuum conditions generated about 0.8 and 16 W/m^2, respectively, as shown in Figure 4e,f.

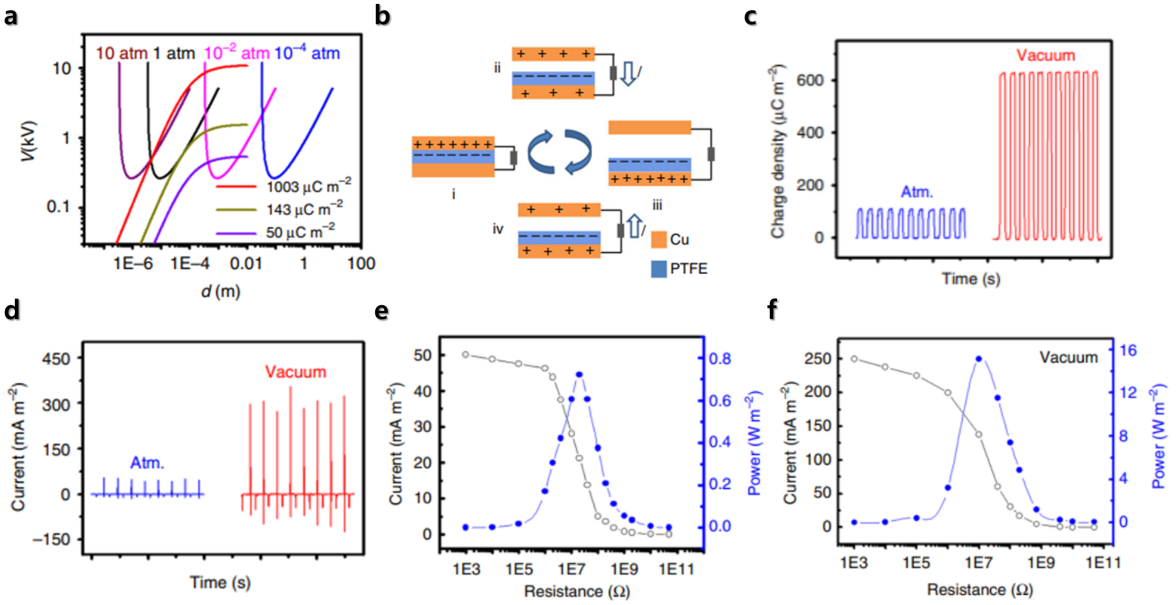

Figure 4. Output enhancement by controlling the atmospheric conditions. (**a**) Air breakdown voltage at different pressures and gap voltage with different charge densities [69]. (**b**) Typical TENG structure used for analysis under vacuum conditions (**c**) Charge density of TENG under air and vacuum. (**d**) Current output of TENG under air and vacuum. (**e**) Current and power outputs of TENG with different resistances. (**f**) Current and power outputs of TENG with different resistances under vacuum conditions.

3. Current Enhancement with Electron Avalanche Effect

As discussed in the previous paragraph, the air breakdown effect is one of the problems that interrupts the TENG output performance because the surface charge can be released through air. However, under certain conditions, this effect can also increase the current output of the TENGs owing to the electron avalanche effect. The electron avalanche effect occurs during the dielectric breakdown within gases, which accelerates electrons by a strong electric field and generates additional electrons by ionizing the gas molecules. In particular, if a strong electric field is generated in air, additional electrons can be generated, as they are also accelerated by the strong electric field. As more charges are transferred, the charge transfer capacity can be increased using the electron avalanche effect; thus, the current output of the TENGs can be increased.

Figure 5 shows previously reported TENGs that can generate a high current output with an air breakdown effect using two metal electrodes. As shown in Figure 5a,b, Chung et al. [70] demonstrated an ion-enhanced field-emission (IEFE)-TENG that can generate a high current output based on electrostatic discharge. Owing to the structure of the IEFE-TENG, electrostatic discharge (ESD) can be generated between the top electrode and the metal-to-metal contact point owing to the charges induced by the dielectric layer. As shown in Figure 5c, ESD was also observed during operation of the IEFE-TENG. Through the electron avalanche effect of this ESD-based electrical output, IEFE-TENG generated a high peak current output of 100–250 mA. The average power of the IEFE-TENG is 635% higher than that of a typical TENG device owing to the electron avalanche effect.

As shown in Figure 5f, Chung et al. [71] demonstrated an ion-gate-based static discharge generator (ISDG) that can generate an ESD-based high-current output. In this study, the TENG device was connected to the ion gate, which can induce ESD through two electrodes; therefore, the ESD-based electrical output was generated through the ion gate. Consequently, the peak current output was increased to 2.5 A by connecting the ion gate to the TENG device, as shown in Figure 5g. In addition, researchers measured the transferred charge of the TENG device with and without an ion-gate and with and without an inductor. Consequently, the transferred charge significantly increased with the ion gate and inductor. The researchers stated that the ESD-based electrical output had a short peak current signal; therefore, it could not capture every signal owing to the low sample measurement rate of the instrument. To solve this issue, they included an inductor to smooth the current waveform so that the measurement instrument could capture each current signal. Because additional charge cannot be produced using only the inductor, this result shows that the transferred charge of the TENG device can be increased by the ESD effect owing to the electron avalanche effect.

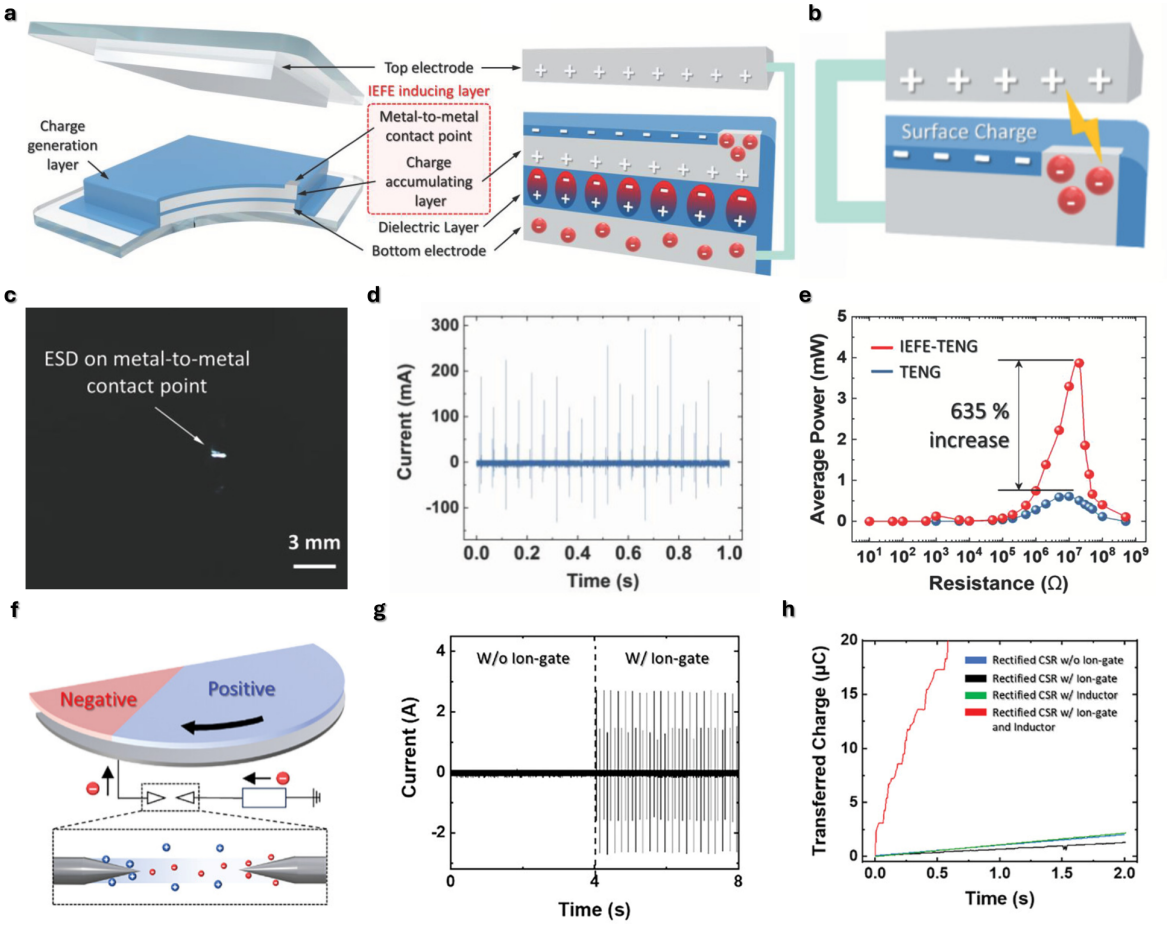

Figure 5. Metal-to-metal ESD-based TENGs. (**a**) Schematic of IEFE-TENG structure [70], Copyright 2019, John Wiley and Sons. (**b**) Schematic of working mechanism of IEFE-TENG. (**c**) Photograph of ESD on metal-to-metal contact point of IEFE-TENG. (**d**) Current output of IEFE-TENG. (**e**) Average power of IEFE-TENG and typical TENG. (**f**) Schematic of ISDG structure and working mechanism [71]. (**g**) Current output of ISDG. (**h**) Transferred charge of ISDG with and without ion gate and inductor.

Figure 6 shows devices that generate current-output-based TENGs by performing ESD directly from the surface charge of the dielectric film. Jianjun et al. [72] developed a direct-current TENG (DC-TENG) that can generate an electrical output via ESD directly from the surface charge of the triboelectric layer, as shown in Figure 6a. As shown in Figure 6b, when the upper substrate slides on the bottom substrate, a surface charge is generated by the contact between the top electrode and the PTFE film and is transferred to the top electrode through the air gap with ESD. Consequently, the device generated a high DC current output via the ESD effect, as shown in Figure 6c.

As shown in Figure 6d, Yoon et al. [73] demonstrated an ESD-based DC-TENG that generated an electrical output by accumulating charges between the charge-conveying layer (CCL) and triboelectric layer. The CCL was constructed using styrene–butadiene rubber (SBR), which is a neutral triboelectric layer. Cross-linked (CL)-PTFE was used as the negative triboelectric layer, and butylated melamine formaldehyde was used as the positive triboelectric layer. An air gap exists between the electrode and CCL to generate ESD through air, as shown in Figure 6e. Consequently, the DC-TENG generated a high current output of ~3 mA (Figure 6f). In addition, the current outputs were influenced by the gap distance between the CCL and electrode, as shown in Figure 6g.

Figure 7 shows ESD-based TENGs with complicated mechanical designs for better energy harvesting. As shown in Figure 7a, Chung et al. [74] demonstrated a film-capacitor-based charge-carrier TENG (FCC-TENG) that generated a high power output using a film capacitor structure and spark gap. Film capacitor–wrapped cylinders were used in the FCC-TENG, and these cylinders roll on the triboelectric layer to accumulate charges from triboelectrification. In addition, a spark gap was used to generate ESD based on the accumulated charges, as shown in Figure 7b. Consequently, the FCC-TENG generated current and voltage outputs of up to 15 A and 6000 V, as shown in Figure 7d,e, respectively.

Figure 7f shows a wind energy–harvesting TENG that can generate a high power output with the ESD effect. Chung et al. demonstrated a wind-driven TENG-connected ambient air ionizing channel (AAIC) that can generate an ESD-based electrical output with a wind input. The device consists of a dielectric film, electrodes, and

poly(methyl methacrylate) substrate, as shown in Figure 7f, so when the wind blows to the device, the film at the middle of the device vibrates between the top and bottom electrodes. Consequently, the dielectric film contacts and separates the top and bottom electrodes; thus, it can induce charges inside the electrodes. As shown in Figure 7g, with the optimized geometry, the film simultaneously contacted the top electrode and separated from the bottom electrode. Consequently, opposite charges were induced inside the electrodes, generating a high-power output through the AAIC. As shown in Figure 7h, the device generated a high current output of up to 4 A using the AAIC. With a high power output, the device was able to charge the supercapacitor, as shown in Figure 7i, and use it as a power source for the electrolysis system to produce hydrogen, as shown in Figures 7j,k. With this output, ~360 μL/h of hydrogen was produced from the electrical output of the TENG device with AAIC while the general fluttering TENG produced ~90 μL/h of hydrogen. These results show that the electron avalanche effect caused by electrostatic discharge can effectively enhance the current output of TENG devices.

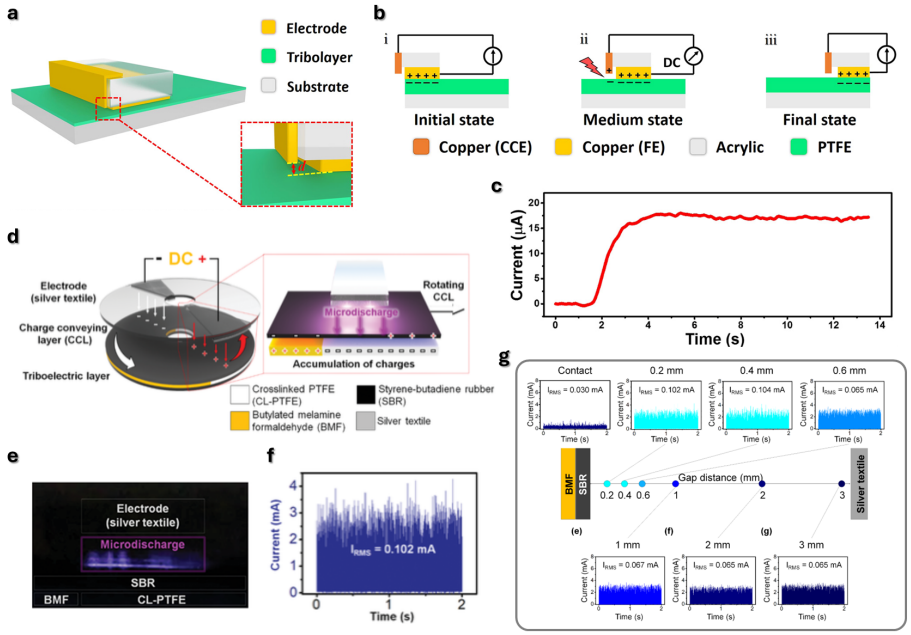

Figure 6. Dielectric film to metal ESD-based TENGs. (**a**) Schematic of DC-TENG with dielectric film–based ESD [72], Copyright 2019, The American Association for the Advancement of Science. (**b**) Working mechanism of DC-TENG with dielectric film–based ESD. (**c**) Current output of DC-TENG with dielectric film–based ESD. (**d**) Schematic of DC-TENG with CCL [73], Copyright 2020, John Wiley and Sons. (**e**) Photograph of microdischarge generated in DC-TENG with CCL. (**f**) Current output of DC-TENG with CCL. (**g**) Current outputs of DC-TENG with CCL with varying gap distances.

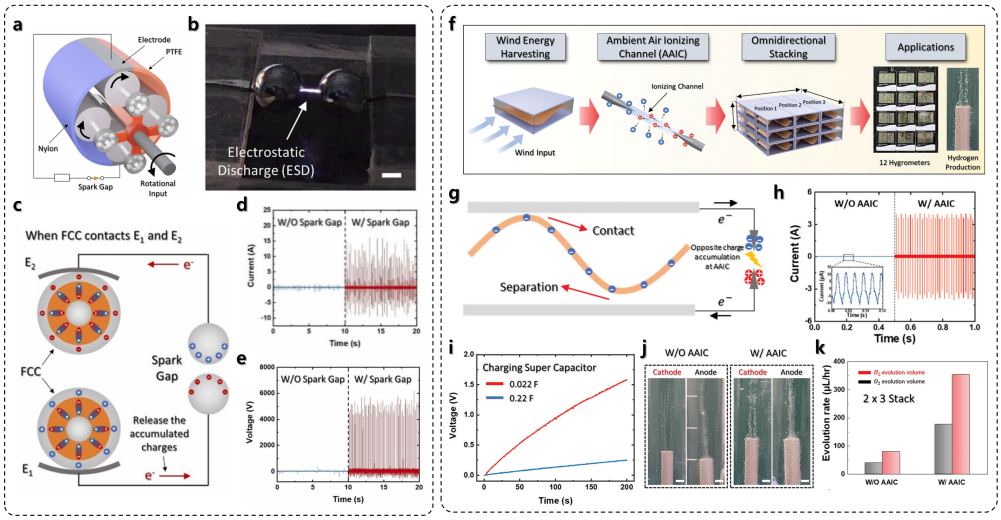

Figure 7. ESD-based TENGs with complicated mechanical designs. (**a**) Schematic of FCC-TENG [74], Copyright 2022, Elsevier. (**b**) Photograph of spark gap connected to FCC-TENG. (**c**) Working mechanism of FCC-TENG.

(**d**) Current output of FCC-TENG with and without spark gap. (**e**) Voltage output of FCC-TENG with and without spark gap. (**f**) Schematics of wind-driven TENG with AAIC [75], Copyright 2023, John Wiley and Sons. (**g**) Working mechanism of wind-driven TENG with AAIC. (**h**) Current output of wind-driven TENG with and without AAIC. (**i**) Charging graph of supercapacitor with wind-driven TENG with AAIC. (**j**) Photographs of electrolysis system operated by wind-driven TENG with and without AAIC. (**k**) Evolution rate of hydrogen and oxygen with electrolysis system operated by wind-driven TENG with and without AAIC.

4. Summary and Perspectives

In this review, we discuss several current amplification strategies for TENGs. To improve the surface charge density of the triboelectric layers of TENGs, the surrounding environment can be controlled by utilizing liquid lubricants or regulating atmospheric conditions, such as vacuum or oxygen conditions. Using these strategies, the air breakdown effect, which releases the surface charge of the triboelectric layers through the air, can be reduced. In addition, to increase the charge transfer capacity of TENGs, strategies using ESD-based electrical output for TENGs have been introduced. Owing to the electron avalanche effect of the ESD-based electrical output, TENGs can generate a current output not only from electrostatic induction but also from the air breakdown effect. Consequently, milliampere-to-ampere-scale peak current outputs were generated using these strategies. Table 1 summarizes the maximum peak voltage, peak current, average power, and peak power of the TENGs described in this review.

Table 1. Comparison of electrical outputs of tengs based on regulating surrounding conditions and utilizing electron avalanche effect.

	Ref.	Peak Voltage (V)	Peak Current (A)	Average Power (W)	Peak Power (W)
Regulating Surrounding Conditions of TENGs	Zhou et al. [66]	450	1.5×10^{-4}	-	0.0329
	Chung et al. [67]	200	0.085	0.00173	0.6
	Wu et al. [68]	470	1.7×10^{-6}	-	-
	Wang et al. [69]	180	4.47×10^{-5}	-	0.00393
Utilizing Electron Avalanche Effect	Chung et al. [70]	466	0.25	0.0039	0.5
	Chung et al. [71]	1500	4	0.169	-
	Liu et al. [72]	750	1.7×10^{-5}	0.01	-
	Yoon et al. [73]	1300	1.03×10^{-4}	0.199	-
	Chung et al. [74]	5000	10	0.720	-
	Son et al. [75]	1400	4	4.25	-

Despite these advances, several challenges remain for the practical deployment of high-current TENG. Additional quantitative studies are required, as follows:

(1) Further design optimization of liquid-lubricant-based and gas-controlled TENGs for practical applications
(2) Further quantitative analysis of the relationship between TENG performance and surrounding environmental conditions, such as liquid properties (e.g., viscosity), gas composition, and ambient temperature
(3) Measurement and practical integration with energy storage for ultrashort and high-current discharge signals of ESD-based electrical output
(4) Long-term effects of ESD-based TENGs on the mechanical lifespan owing to surface carbonization.

With these additional quantitative studies, we believe that the research scope can be further expanded by combining multiple current-amplification strategies, for example, through the use of controlled gaseous environments such as CO_2 or SF_6. Moreover, these advances may broaden the application fields of TENGs, particularly for space-related technologies, including spacecraft and Mars exploration, owing to their adaptability to various atmospheric conditions.

We hope that researchers working on triboelectric nanogenerators will benefit from the strategies and challenges summarized in this review. We believe that this study will serve as a useful guide for designing high-current TENGs and promote further studies toward practical applications.

Author Contributions

S.-H.C. and S.L.: conceptualization; S.-H.C.: visualization; S.L.: supervision; S.-H.C. and S.L.: writing—original draft preparation; S.-H.C. and S.L.: writing—reviewing and editing. All authors have read and agreed to the published version of the manuscript.

Funding

This work was supported by the National Research Foundation of Korea (NRF) grant, funded by the Korea government (MSIT) (Nos.2023R1A2C2006170 and RS-2025-02214162).

Institutional Review Board Statement

Not applicable.

Informed Consent Statement

Not applicable.

Data Availability Statement

Not applicable.

Conflicts of Interest

Given the role as Editorial Board Member, Sangmin Lee had no involvement in the peer review of this paper and had no access to information regarding its peer-review process. Full responsibility for the editorial process of this paper was delegated to another editor of the journal.

Use of AI and AI-Assisted Technologies

No AI tools were utilized for this paper.

References

1. Fan, F.-R.; Tian, Z.-Q.; Wang, Z.L. Flexible Triboelectric Generator. *Nano Energy* **2012**, *1*, 328–334. https://doi.org/10.1016/j.nanoen.2012.01.004.
2. Wu, C.; Wang, A.C.; Ding, W.; et al. Triboelectric Nanogenerator: A Foundation of the Energy for the New Era. *Adv. Energy Mater.* **2019**, *9*, 1802906. https://doi.org/10.1002/aenm.201802906.
3. Wang, Y.; Yang, Y.; Wang, Z.L. Triboelectric Nanogenerators as Flexible Power Sources. *NPJ Flex. Electron.* **2017**, *1*, 10. https://doi.org/10.1038/s41528-017-0007-8.
4. Wang, Z.L. Triboelectric Nanogenerators as New Energy Technology for Self-Powered Systems and as Active Mechanical and Chemical Sensors. *ACS Nano* **2013**, *7*, 9533–9557. https://doi.org/10.1021/nn404614z.
5. Chung, S.-H.; Kim, M.; Lin, Z.-H.; et al. Enhancing Strategy of Triboelectric Nanogenerator via Origami Pattern by Harvesting Mechanical Motion and Wind Flow. *Int. J. Energy Res.* **2024**, *2024*, 2120442. https://doi.org/10.1155/2024/2120442.
6. Xing, F.; Gao, X.; Gao, W.; et al. High-Entropy Energy for Self-Powered Systems. *SmartSys* **2025**, *1*, e70001. https://doi.org/10.1002/sys3.70001.
7. Li, X.; Wang, Z.L.; Wei, D. Iontronic Logic Control Driven by Dynamic Electrical Double Layer Regulation. *Iontronics* **2025**, *1*, 2. https://doi.org/10.20517/iontronics.2025.02.
8. Briscoe, J.; Dunn, S. Piezoelectric Nanogenerators–A Review of Nanostructured Piezoelectric Energy Harvesters. *Nano Energy* **2015**, *14*, 15–29. https://doi.org/10.1016/j.nanoen.2014.11.059.
9. Wang, Z.L.; Song, J. Piezoelectric Nanogenerators Based on Zinc Oxide Nanowire Arrays. *Science* **2006**, *312*, 242–246. https://doi.org/10.1126/science.1124005.
10. Xu, Q.; Wen, J.; Qin, Y. Development and Outlook of High Output Piezoelectric Nanogenerators. *Nano Energy* **2021**, *86*, 106080. https://doi.org/10.1016/j.nanoen.2021.106080.
11. Zhang, D.; Wang, Y.; Yang, Y. Design, Performance, and Application of Thermoelectric Nanogenerators. *Small* **2019**, *15*, 1805241. https://doi.org/10.1002/smll.201805241.
12. Feng, R.; Tang, F.; Zhang, N.; et al. Flexible, High-Power Density, Wearable Thermoelectric Nanogenerator and Self-Powered Temperature Sensor. *ACS Appl. Mater. Interfaces* **2019**, *11*, 38616–38624. https://doi.org/10.1021/acsami.9b11435.
13. Kim, A.; Kumar, P.; Annamalai, P.K.; et al. Recent Advances in the Nanomaterials, Design, Fabrication Approaches of Thermoelectric Nanogenerators for Various Applications. *Adv. Mater. Interfaces* **2022**, *9*, 2201659. https://doi.org/10.1002/admi.202201659.
14. Jee, M.; Cha, K.; Chung, S.H.; et al. Contamination-Resilient, High-Output Triboelectric Nanogenerator with Fully-Recycled, Multi-Material Crumpled Balls. *EcoMat* **2025**, *7*, e70040. https://doi.org/10.1002/eom2.70040.
15. Chung, S.-H.; Jang, Y.H.; Kim, D.; et al. High-Output Wearable Flow Ring-Based Triboelectric Nanogenerator via Opposite Charging Intermediate Layer. *Int. J. Energy Res.* **2023**, *2023*, 3415211. https://doi.org/10.1155/2023/3415211.

16. Cha, K.; In, S.; Chung, S.H.; et al. Improving Electrical Performance and Lifespan of Liquid-Based Triboelectric Nanogenerator via Charge-Inducing Structure. *Adv. Funct. Mater.* **2025**, *35*, 2505695. https://doi.org/10.1002/adfm.202505695.
17. Hur, J.; Song, M.; Yong, H.; et al. Human-Driven Triboelectric Nanogenerator via Simultaneous Harvesting of Body-Coupled Energy. *Nano Energy* **2025**, *135*, 110645. https://doi.org/10.1016/j.nanoen.2025.110645.
18. Heo, D.; Hur, J.; Lee, S.; et al. Commercial Soccer Ball-Integrated Triboelectric Nanogenerator. *Adv. Eng. Mater.* **2024**, *26*, 2400134. https://doi.org/10.1002/adem.202400134.
19. Son, J.H.; Heo, D.; Goh, D.; et al. Wind-Driven Bidirectional Fluttering Triboelectric Nanogenerator via Dual Flagpole and Slot Structure Design. *Adv. Mater. Technol.* **2023**, *8*, 2200453. https://doi.org/10.1002/admt.202200453.
20. Song, M.; Hur, J.; Heo, D.; et al. Current Amplification through Deformable Arch-Shaped Film Based Direct-Current Triboelectric Nanogenerator for Harvesting Wind Energy. *Appl. Energy* **2023**, *344*, 121248. https://doi.org/10.1016/j.apenergy.2023.121248.
21. Heo, D.; Hur, J.; Cho, H.; et al. Nano-Oil-Barrier-Based Fluttering Triboelectric Nanogenerator. *Adv. Sci.* **2025**, *12*, e02278. https://doi.org/10.1002/advs.202502278.
22. Jeon, H.; Cha, K.; Jee, M.; et al. End-Linked Multistrip-Flutter Triboelectric Nanogenerator for Enhanced Electrostatic Discharge Output and Frequency. *Nano Energy* **2025**, *147*, 111584. https://doi.org/10.1016/j.nanoen.2025.111584.
23. Chen, B.; Yang, Y.; Wang, Z.L. Scavenging Wind Energy by Triboelectric Nanogenerators. *Adv. Energy Mater.* **2018**, *8*, 1702649. https://doi.org/10.1002/aenm.201702649.
24. Hasan, M.A.M.; Zhu, W.; Bowen, C.R.; et al. Triboelectric Nanogenerators for Wind Energy Harvesting. *Nat. Rev. Electr. Eng.* **2024**, *1*, 453–465. https://doi.org/10.1038/s44287-024-00061-6.
25. Chung, S.-H.; Chung, J.; Kim, B.; et al. Screw Pump-Type Water Triboelectric Nanogenerator for Active Water Flow Control. *Adv. Mater. Technol.* **2021**, *23*, 2000758. https://doi.org/10.1002/adem.202000758.
26. Kim, T.; Kim, D.Y.; Yun, J.; et al. Direct-Current Triboelectric Nanogenerator via Water Electrification and Phase Control. *Nano Energy* **2018**, *52*, 95–104. https://doi.org/10.1016/j.nanoen.2018.07.048.
27. Wang, Z.L.; Jiang, T.; Xu, L. Toward the Blue Energy Dream by Triboelectric Nanogenerator Networks. *Nano Energy* **2017**, *39*, 9–23. https://doi.org/10.1016/j.nanoen.2017.06.035.
28. Rodrigues, C.; Nunes, D.; Clemente, D.; et al. Emerging Triboelectric Nanogenerators for Ocean Wave Energy Harvesting: State of the Art and Future Perspectives. *Energy Environ. Sci.* **2020**, *13*, 2657–2683. https://doi.org/10.1039/D0EE01258K.
29. Xie, Y.; Wang, S.; Niu, S.; et al. Multi-Layered Disk Triboelectric Nanogenerator for Harvesting Hydropower. *Nano Energy* **2014**, *6*, 129–136. https://doi.org/10.1016/j.nanoen.2014.03.015.
30. Wang, S.; Li, H.; Jia, L.; et al. A High-Performance, High-Impedance Ratio, Bidirectional Charge Transferred Triboelectric Nanogenerators System. *Adv. Funct. Mater.* **2025**, e29059. https://doi.org/10.1002/adfm.202529059.
31. Yu, Y.; Li, H.; Zhang, X.; et al. Substantially Boosting Performance of Triboelectric Nanogenerators via a Triboelectrification Enhancement Effect. *Joule* **2024**, *8*, 1855–1868. https://doi.org/10.1016/j.joule.2024.04.013.
32. Cho, S.; Cha, K.; Kim, B.; et al. Sustainable Utilization of Aging-Deteriorated Microplastics as Triboelectric Nanogenerator. *Chem. Eng. J.* **2023**, *470*, 144283. https://doi.org/10.1016/j.cej.2023.144283.
33. Yu, Y.; Li, H.; Zhao, D.; et al. Material's Selection Rules for High Performance Triboelectric Nanogenerators. *Mater. Today* **2023**, *64*, 61–71. https://doi.org/10.1016/j.mattod.2023.03.008.
34. Ahn, J.; Kim, J.S.; Jeong, Y.; et al. All-Recyclable Triboelectric Nanogenerator for Sustainable Ocean Monitoring Systems. *Adv. Energy Mater.* **2022**, *12*, 2201341. https://doi.org/10.1002/aenm.202201341.
35. Cha, K.; Chung, J.; Heo, D.; et al. Lightweight Mobile Stick-Type Water-Based Triboelectric Nanogenerator with Amplified Current for Portable Safety Devices. *Nano Energy* **2022**, *104*, 107912. https://doi.org/10.1080/14686996.2022.2030195.
36. Chung, S.-H.; Song, M.; Yong, H.; et al. A Loop-Structured Film-Capacitor-Based High-Performance Direct-Current Triboelectric Nanogenerator with Temporary Charge Accumulation. *J. Mater. Chem. A* **2025**, *13*, 17376–17383. https://doi.org/10.1039/D4TA09187F.
37. Li, T.; Xu, Y.; Willander, M.; et al. Lightweight Triboelectric Nanogenerator for Energy Harvesting and Sensing Tiny Mechanical Motion. *Adv. Funct. Mater.* **2016**, *26*, 4370–4376. https://doi.org/10.1002/adfm.201600279.
38. Chung, S.-H.; Jee, M.; Kang, S.; et al. Ultracompact Ball Vibrating Triboelectric Nanogenerator for Maximizing Instantaneous Power Output in Minimized Size. *Int. J. Energy Res.* **2025**, *2025*, 9259935. https://doi.org/10.1155/er/9259935.
39. Son, J.H.; Cha, K.; Chung, S.H.; et al. Recycled, Contaminated, Crumpled Aluminum Foil-Driven Triboelectric Nanogenerator. *Adv. Sci.* **2023**, *10*, 2301609. https://doi.org/10.1002/advs.202301609.
40. Li, Y.; Zhao, Z.; Gao, Y.; et al. Low-Cost, Environmentally Friendly, and High-Performance Triboelectric Nanogenerator Based on a Common Waste Material. *ACS Appl. Mater. Interfaces* **2021**, *13*, 30776–30784. https://doi.org/10.1021/acsami.1c09192.
41. Hu, S.; Weber, J.; Chang, S.; et al. A Low-Cost Simple Sliding Triboelectric Nanogenerator for Harvesting Energy from Human Activities. *Adv. Mater. Technol.* **2022**, *7*, 2200186. https://doi.org/10.1002/admt.202200186.

42. Hwang, H.J.; Kwon, D.; Kwon, H.Y.; et al. Integrated System of Mechanical Regulator and Electrical Circuitry on Triboelectric Energy Harvesting with Near-Field Communication for Low Power Consumption. *Adv. Energy Mater.* **2024**, *15*, 2400481. https://doi.org/10.1002/aenm.202400481.
43. Zi, Y.; Guo, H.; Wen, Z.; et al. Harvesting Low-Frequency (<5 Hz) Irregular Mechanical Energy: A Possible Killer Application of Triboelectric Nanogenerator. *ACS Nano* **2016**, *10*, 4797–4805. https://doi.org/10.1021/acsnano.6b01569.
44. Ahmed, A.; Hassan, I.; Helal, A.S.; et al. Triboelectric Nanogenerator versus Piezoelectric Generator at Low Frequency (<4 Hz): A Quantitative Comparison. *iScience* **2020**, *23*, 101340. https://doi.org/10.1016/j.isci.2020.101286.
45. Yu, Y.; Gao, Q.; Zhang, X.; et al. Contact-Sliding-Separation Mode Triboelectric Nanogenerator. *Energy Environ. Sci.* **2023**, *16*, 3932–3941. https://doi.org/10.1039/D3EE01290E.
46. Wang, C.; Wang, P.; Chen, J.; et al. Self-Powered Biosensing System Driven by Triboelectric Nanogenerator for Specific Detection of Gram-Positive Bacteria. *Nano Energy* **2022**, *93*, 106828. https://doi.org/10.1016/j.nanoen.2021.106828.
47. Zhang, H.; Yang, Y.; Hou, T.-C.; et al. Triboelectric Nanogenerator Built inside Clothes for Self-Powered Glucose Biosensors. *Nano Energy* **2013**, *2*, 1019–1024. https://doi.org/10.1016/j.nanoen.2013.03.024.
48. Lu, W.; Wang, X.; Wang, C.; et al. A Self-Powered Biosensor Based on Triboelectric Nanogenerator for Dual-Specificity Bacterial Detection. *InfoMat* **2024**, *6*, e12508. https://doi.org/10.1002/inf2.12508.
49. Hwang, H.J.; Kim, J.S.; Oh, S.; et al. Self-Powered Real-Time Temperature Sensing Based on Flexible Ionic Elastomer on Triboelectric Nanogenerators. *Adv. Funct. Mater.* **2025**, *35*, e04081. https://doi.org/10.1002/adfm.202504081.
50. Kang, S.; Heo, D.; Chung, S.H.; et al. Exhalation-Driven Mask-Valve-Integrated Triboelectric Nanogenerator with Amplified Output Current. *Small Struct.* **2025**, *6*, e202500280. https://doi.org/10.1002/sstr.202500280.
51. Zou, Y.; Xu, J.; Fang, Y.; et al. A Hand-Driven Portable Triboelectric Nanogenerator Using Whirligig Spinning Dynamics. *Nano Energy* **2021**, *83*, 105845. https://doi.org/10.1016/j.nanoen.2021.105845.
52. Chung, J.; Yong, H.; Moon, H.; et al. Hand-Driven Gyroscopic Hybrid Nanogenerator for Recharging Portable Devices. *Adv. Mater. Technol.* **2018**, *5*, 1801054. https://doi.org/10.1002/advs.201801054.
53. Heo, D.; Chung, J.; Kim, B.; et al. Triboelectric Speed Bump as a Self-Powered Automobile Warning and Velocity Sensor. *Nano Energy* **2020**, *72*, 104719. https://doi.org/10.1016/j.nanoen.2020.104719.
54. Heo, D.; Song, M.; Chung, S.H.; et al. Inhalation-Driven Vertical Flutter Triboelectric Nanogenerator with Amplified Output as a Gas-Mask-Integrated Self-Powered Multifunctional System. *Adv. Energy Mater.* **2022**, *12*, 2201001. https://doi.org/10.1002/aenm.202201001.
55. Heo, D.; Song, M.; Bae, J.; et al. Self-Powered Emergency Response Gas-Mask-System via Multi-Dielectric Flutter with Negligible Inhalation Resistance. *Chem. Eng. J.* **2024**, *499*, 156349. https://doi.org/10.1016/j.cej.2024.156349.
56. Jung, Y.; Yu, J.; Hwang, H.J.; et al. Wire-Based Triboelectric Resonator for a Self-Powered Crack Monitoring System. *Nano Energy* **2020**, *71*, 104615. https://doi.org/10.1016/j.nanoen.2020.104615.
57. Shao, J.; Jiang, T.; Wang, Z.L. Theoretical Foundations of Triboelectric Nanogenerators (TENGs). *Sci. China Technol. Sci.* **2020**, *63*, 1087–1109. https://doi.org/10.1007/s11431-020-1604-9.
58. Jiang, C.; Dai, K.; Yi, F.; et al. Optimization of Triboelectric Nanogenerator Load Characteristics Considering the Air Breakdown Effect. *Nano Energy* **2018**, *53*, 706–715. https://doi.org/10.1016/j.nanoen.2018.09.036.
59. Saurenbach, F.; Wollmann, D.; Terris, B.; et al. Force Microscopy of Ion-Containing Polymer Surfaces: Morphology and Charge Structure. *Langmuir* **1992**, *8*, 1199–1203. https://doi.org/10.1021/la00040a030.
60. Shin, E.-C.; Ko, J.-H.; Lyeo, H.-K.; et al. Derivation of a Governing Rule in Triboelectric Charging and Series from Thermoelectricity. *Phys. Rev. Res.* **2022**, *4*, 023131. https://doi.org/10.1103/PhysRevResearch.4.023131.
61. Xu, C.; Zi, Y.; Wang, A.C.; et al. On the Electron-Transfer Mechanism in the Contact-Electrification Effect. *Adv. Mater.* **2018**, *30*, 1706790. https://doi.org/10.1002/adma.201706790.
62. Willatzen, M.; Wang, Z.L. Contact Electrification by Quantum-Mechanical Tunneling. *Research* **2019**, *2019*, 6528789. https://doi.org/10.34133/2019/6528689.
63. Zou, H.; Zhang, Y.; Guo, L.; et al. Quantifying the Triboelectric Series. *Nat. Commun.* **2019**, *10*, 1427. https://doi.org/10.1038/s41467-019-09461-x.
64. Zou, H.; Guo, L.; Xue, H.; et al. Quantifying and Understanding the Triboelectric Series of Inorganic Non-Metallic Materials. *Nat. Commun.* **2020**, *11*, 2093. https://doi.org/10.1038/s41467-020-15926-1.
65. Zi, Y.; Wu, C.; Ding, W.; et al. Maximized Effective Energy Output of Contact-Separation-Triggered Triboelectric Nanogenerators as Limited by Air Breakdown. *Adv. Funct. Mater.* **2017**, *27*, 1700049. https://doi.org/10.1002/adfm.201700049.
66. Zhou, L.; Liu, D.; Zhao, Z.; et al. Simultaneously Enhancing Power Density and Durability of Sliding-Mode Triboelectric Nanogenerator via Interface Liquid Lubrication. *Adv. Energy Mater.* **2020**, *10*, 2002920. https://doi.org/10.1002/aenm.202002920.
67. Chung, S.H.; Chung, J.; Song, M.; et al. Nonpolar Liquid Lubricant Submerged Triboelectric Nanogenerator for Current Amplification via Direct Electron Flow. *Adv. Energy Mater.* **2021**, *11*, 2100936. https://doi.org/10.1002/aenm.202100936.

68. Wu, J.; Xi, Y.; Shi, Y. Toward Wear-Resistive, Highly Durable and High Performance Triboelectric Nanogenerator through Interface Liquid Lubrication. *Nano Energy* **2020**, *72*, 104659. https://doi.org/10.1016/j.nanoen.2020.104659.
69. Wang, J.; Wu, C.; Dai, Y.; et al. Achieving Ultrahigh Triboelectric Charge Density for Efficient Energy Harvesting. *Nat. Commun.* **2017**, *8*, 88. https://doi.org/10.1038/s41467-017-00131-4.
70. Chung, J.; Heo, D.; Shin, G.; et al. Ion-Enhanced Field Emission Triboelectric Nanogenerator. *Adv. Energy Mater.* **2019**, *9*, 1901731. https://doi.org/10.1002/aenm.201901731.
71. Chung, S.H.; Hur, J.; Kim, S.; et al. Reaching New Efficiency Milestones in Low-Speed Wind Energy Harvesting via Noncontact Stackable Ion-Gate-Based Static Discharge Generator. *Adv. Energy Mater.* **2025**, *15*, 2500033. https://doi.org/10.1002/aenm.202500033.
72. Liu, D.; Yin, X.; Guo, H.; et al. A Constant Current Triboelectric Nanogenerator Arising from Electrostatic Breakdown. *Sci. Adv.* **2019**, *5*, eaav6437. https://doi.org/10.1126/sciadv.aav6437.
73. Yoon, H.J.; Kang, M.; Seung, W.; et al. Microdischarge-Based Direct Current Triboelectric Nanogenerator via Accumulation of Triboelectric Charge in Atmospheric Condition. *Adv. Energy Mater.* **2020**, *10*, 2000730. https://doi.org/10.1002/aenm.202000730.
74. Chung, S.-H.; Cha, K.; Song, M.; et al. Sub-Watt Power Triboelectric Generator via Polarization Switching Charge Carrier. *Nano Energy* **2022**, *103*, 107754. https://doi.org/10.1016/j.nanoen.2022.107754.
75. Son, J.H.; Chung, S.H.; Cha, K.; et al. Ultrahigh Performance, Serially Stackable, Breeze Driven Triboelectric Generator via Ambient Air Ionizing Channel. *Adv. Mater.* **2023**, *35*, 2300283. https://doi.org/10.1002/adma.202300283.